Results in Physics 39 (2022) 105740

Contents lists available at ScienceDirect

Results in Physics

journal homepage: www.elsevier.com/locate/rinp

Reconfigurable high-Q terahertz filtering of VO_2-based metamaterials using optical tunneling

Xueying Liu [a,b], Yinong Xie [a], Wei Chen [a], Sayed Ali Khan [a], Jun Zhou [c], Jinlin Qiu [a,b], Jinfeng Zhu [a,b,*]

[a] Institute of Electromagnetics and Acoustics and Key Laboratory of Electromagnetic Wave Science and Detection Technology, Xiamen University, Xiamen 361005, China
[b] State Key Laboratory of Applied Optics, Changchun Institute of Optics, Fine Mechanics and Physics, Chinese Academy of Sciences, Changchun 130033, China
[c] Terahertz Research Center, University of Electronic Science and Technology of China, Chengdu 610054, China

ARTICLE INFO

Keywords:
Metamaterial
Filter
Vanadium dioxide
Optical tunneling

ABSTRACT

Up to date, reconfigurable terahertz (THz) band-pass filters based on the design of metamaterials with vanadium dioxide (VO_2) have been investigated extensively. However, VO_2-based THz metamaterials with high-quality tunable narrowband transmission and good stop-band rejection have yet to be reported, which are essential for THz wave filtering components or systems. Here, we propose a reconfigurable filter in combination with a dielectric metastructure and a VO_2 thin film. Utilizing the optical tunneling effects of a cavity layer, the filter has a high band-pass transmission up to 98% at 0.246 THz with a narrow bandwidth of 0.0009 THz, an ultra-high Q-factor of 273, and two broad nearly-suppressed sidebands. The transmission intensity can be modulated by the phase transition of VO_2, and the modulation depth is as high as 96.4%. By efficiently tuning the cavity layer thickness, the filter can be designed for a series of transmission wavelengths and further accomplish the switch between the narrow band-pass filtering and wideband reflection. Moreover, the manipulation of the incident angle and polarization can be adopted as an additional degree to achieve a similar switching function. Our study implies a potential for developing various THz applications, where reconfigurable high-Q THz filtering is required.

Introduction

Terahertz (THz) waves with the wavelengths in the range of 30–3000 μm have attracted significant research attention in recent decades due to their potential applications in biosensing, security detection, imaging, spectroscopy, and communications [1–5]. Along with the development of integrated THz systems, high-performance band-pass filters have become essential [6–8]. In the past few years, THz filters based on metamaterials (MMs) have been intensively studied [9–12] because MMs provide a powerful tool to boost the filtering performance. Typically, these filters are passive and do not support active modulation, limiting their application in various THz fields.

Recently, VO_2 provides a good opportunity to develop active THz devices. It is a phase change material with unique optical and electrical switching properties due to the insulator-to-metal transition (IMT) around the temperature of ~ 67 °C [13]. The transmission intensity of the THz wave can be actively modulated through the dramatic change in the conductivity of VO_2 (five orders of magnitude). Up to date, a variety of advanced filters based on the combination of MMs and VO_2 have been investigated [14–20]. Hu et al. have studied a reconfigurable band-pass filter of VO_2-based MMs by voltage tuning, and the transmission could be modulated from 90% to 1% with the full width at half maximum (FWHM) of 0.38 THz [14]. Similarly, by applying a DC-bias voltage to the VO_2 film under a patterning slot antenna, Gyun et al. have observed a 30% THz modulation [15]. Shin et al. have proposed an electrically controllable square-loop MM based on a VO_2 film and achieved a transmission with a Q-factor of 2.37 at the center frequencies of 0.47 THz [16]. However, the use of metallic materials in these filters usually leads to high insertion loss, which results in broad transmission resonances with low modulation depths and quality factors. Nowadays, the THz MM filters with a reconfigurable ultra-narrow filtering band and ultra-low sidebands are still quite in demand.

In this work, a reconfigurable narrowband filter based on the dielectric MM is designed by using the IMT features of VO_2 at THz

* Corresponding author at: Institute of Electromagnetics and Acoustics and Key Laboratory of Electromagnetic Wave Science and Detection Technology, Xiamen University, Xiamen 361005, China.
E-mail address: nanoantenna@hotmail.com (J. Zhu).

https://doi.org/10.1016/j.rinp.2022.105740
Received 2 March 2022; Received in revised form 20 May 2022; Accepted 12 June 2022
Available online 14 June 2022

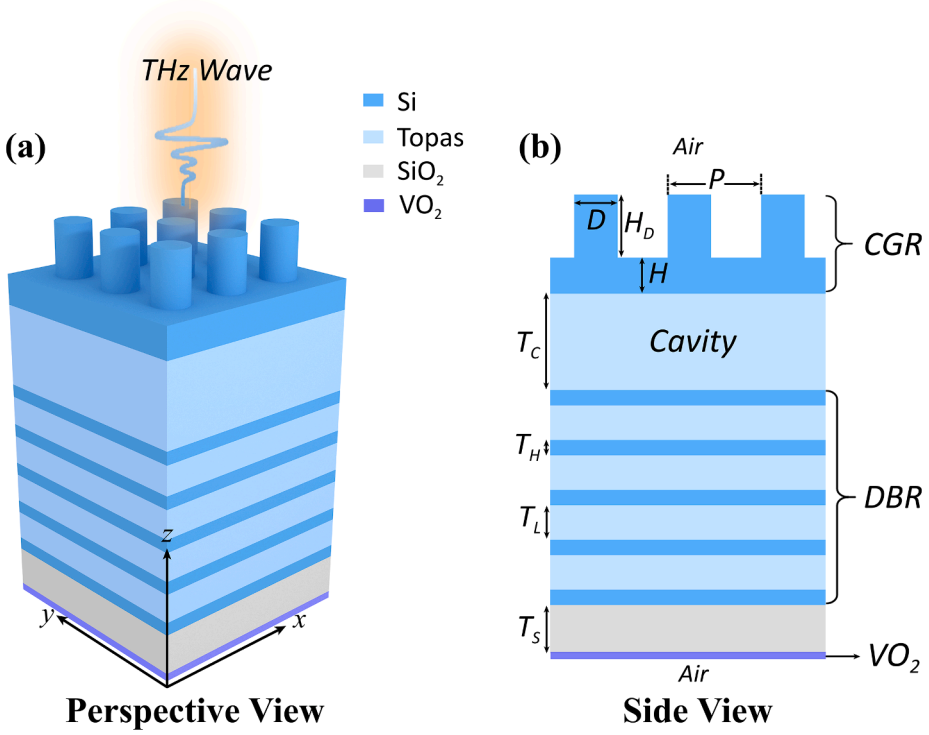

Fig. 1. (a) Schematic drawing of the proposed THz MM device. (b) Side view of the metastructure.

frequencies. When VO_2 is in the low-temperature insulating phase, the MM behaves like a narrowband filter with a high transmission, which is attributed to the optical tunneling effects of the dielectric MM. As the VO_2 layer is switched to the metallic phase, the device blocks all the light in a wide THz band. Unlike other VO_2-based THz MM filters, the proposed filter exhibits unique device performance, including narrowband transmission filtering with an ultra-high Q-factor of 273, a high modulation depth of 96.4%, and good rejection of sidebands. Furthermore, the switch between the narrowband filtering and perfect reflection for the designed MM can be implemented by changing the thickness of a cavity layer. A similar switching function can be achieved by manipulating the incident angle and polarization. The combination of dielectric MM and VO_2 offers an alternative way for developing active miniaturized filters with high-performance reconfigurable THz responses.

Design and method

The proposed structure is illustrated in Fig. 1. The MM consists of a periodic subwavelength silicon (Si) connected grating reflector (CGR), a polyethylene cyclic olefin copolymer (Topas) cavity layer, a distributed Bragg reflector (DBR), a silica (SiO_2) layer, and a VO_2 film layer from top to bottom. We perform optical simulations based on the rigorous coupled-wave analysis (RCWA) for the proposed device and further analyze the field distribution using the finite element method (FEM, COMSOL Multiphysics). In the simulations, periodic boundary conditions are adopted in the *x*- and *y*- directions. The dielectric materials of Si, SiO_2 and Topas are assumed to be nonmagnetic ($\mu = \mu_0$) and their optical parameters are obtained from the references [21,22]. The optical permittivity of VO_2 can be described by the Drude model [13],

$$\varepsilon_{VO_2} = \varepsilon_\infty - \frac{\omega_p^2(\sigma_{VO_2})}{\omega^2 + i\cdot\omega\cdot\gamma} \tag{1}$$

where ε_∞=12 is the relative permittivity at the infinite frequency and $\gamma = 5.75 \times 10^{13}$ s^{-1} is the damping constant. The plasma frequency $\omega_p(\sigma_{VO2})$ as a function of σ_{VO2} can be expressed by,

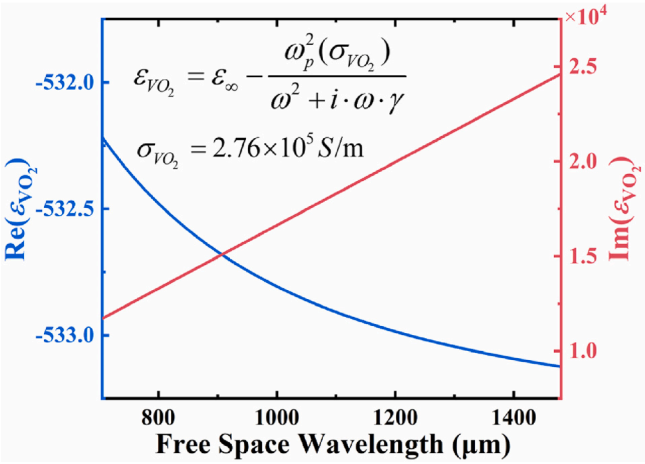

Fig. 2. Dispersive relative permittivity of VO_2 in the THz range.

$$\omega_p(\sigma_{VO_2}) = \frac{\sigma_{VO_2}}{\sigma_0}\cdot\omega_p^2(\sigma_0) \tag{2}$$

where $\sigma_0 = 3 \times 10^5$ S/m is the reference conductivity and $\omega_p(\sigma_0) = 1.4 \times 10^{15}$ s^{-1} is the corresponding plasma frequency of σ_0. In this study, the imitation of the phase-transition of VO_2 is described by changing the conductivity σ_{VO2} from 2.76×10^5 S/m to 0 S/m. The two conductivities correspond to the metallic and insulating phases, respectively. We plot the permittivity dispersion of VO_2 with the conductivity of $\sigma_{VO2} = 2.76 \times 10^5$ S/m in the THz range of interest in Fig. 2. The transition boundary condition is used in the FEM simulation of VO_2 with a thickness of 0.2 μm to reduce the mesh number and simulation time. The period of the unit cell is set as $P = 660$ μm. For the Si CGR, the rod diameter is $D = 394$ μm, the rod height is $H_D = 453$ μm, and the homogeneous layer thickness is $H = 157.5$ μm. The thicknesses of Si and Topas in the DBR structure are $T_H = 67.21$ μm and $T_L = 150.24$ μm, respectively. $T_c = 360$ μm and

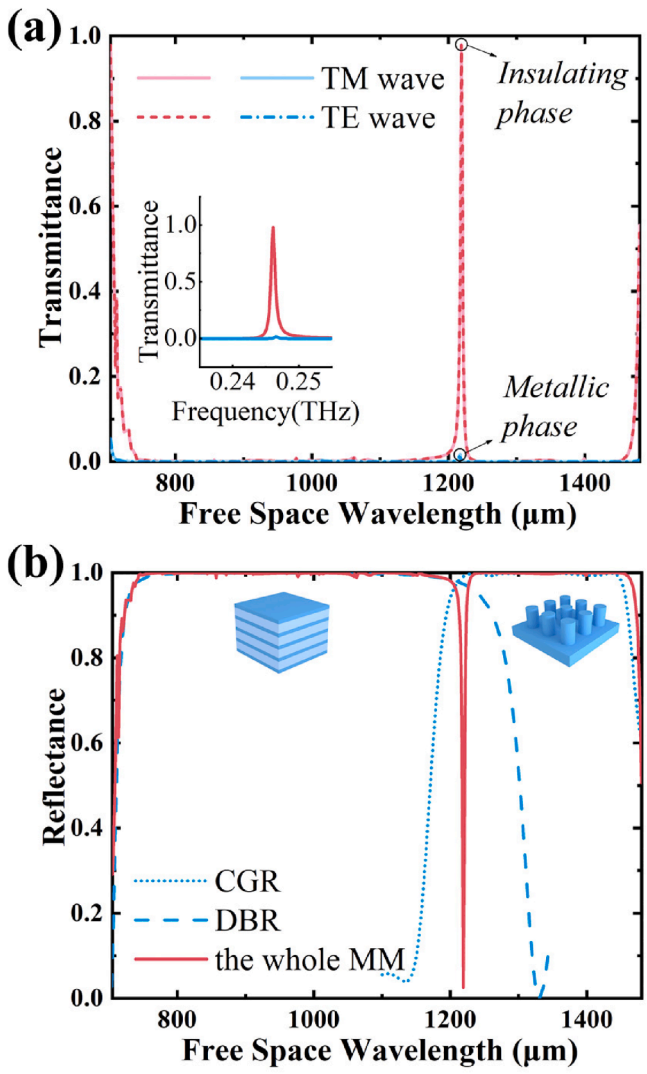

Fig. 3. (a) Simulated transmittance of the THz MM filter for two different VO_2 phases under normal incidence of TE and TM waves, respectively. Inset: detailed spectrum at the peak point. (b) Reflectance for the DBR, CGR and whole MM structure, respectively.

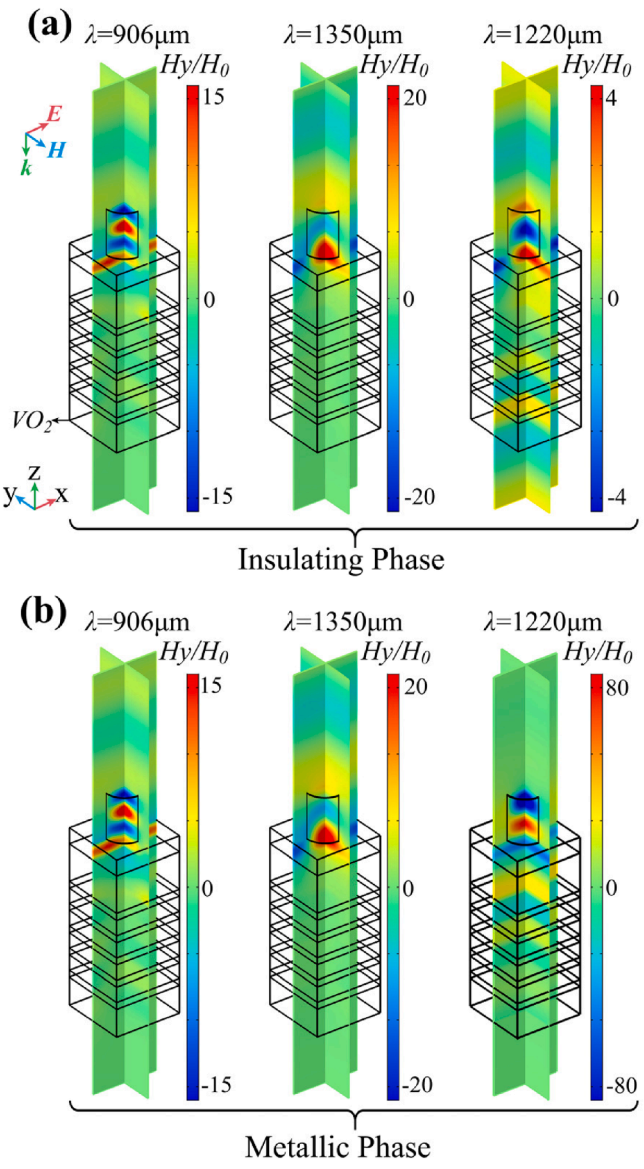

Fig. 4. Normalized magnetic field distributions of the whole MM structure when for two different VO_2 is in the (a) insulating phase and (b) metallic phase, respectively.

$T_s = 273$ μm are the thicknesses of the Topas cavity layer and SiO_2 layer, respectively. The design scheme of CGR and DBR will be discussed in "*Results and discussion*" section.

Results and discussion

Based on the phase transition of VO_2, the transmittance (T) spectra are shown in Fig. 3(a). For the axisymmetric structure, the transmittance spectra for both polarizations are completely the same, which implies a polarization-insensitive property. When VO_2 is in the insulating phase, the spectrum exhibits a sharp resonance peak with the transmittance of 98% at 1220 μm (f_0 = 0.246 THz). The transmission peak has two sidebands with the near-zero transmittance in the wavelength range of 743–1456 μm. This is attributed to the optical tunneling effects in the dielectric MM. The narrow transmission band possesses the FWHM of 0.0009 THz and Q-factor of 273 calculated by $Q = f_0/FWHM$ in the THz range, as observed in the inset of Fig. 3(a). The transition of VO_2 from dielectric to metal induces a considerable reduction of transmittance (as low as 1.6%) at 1220 μm. The intensity modulation depth (M_d) in this study is defined as below [23],

$$M_d = |T_0 - T| \times 100\% \quad (3)$$

where T_0 and T are the maximum transmittance for the insulating and metallic phases of VO_2, respectively. A distinct intensity modulation with $M_d = 96.4\%$ of the narrowband transmission peak can be obtained as a result of the phase transition of VO_2. To reveal the transmission mechanism of the proposed filter, the reflectance (R) spectra of the DBR, CGR, and the whole MM structure are shown in Fig. 3(b). The DBR acts as a wideband perfect reflector in the short wavelength range, with a central wavelength (λ_0) of 921.6 μm, as modeled by the quarter-wave design [24]. The thicknesses of Si and Topas layers for the DBR can be calculated by $\lambda_0/4n$, where n is the refractive index of the corresponding layer. The CGR is originally designed based on the previous work [25], which exhibits a perfect reflection in the long-wavelength range. The low-index cavity layer is used to improve the edge features of the passband by superimposing different reflectors to suppress undesired electromagnetic responses and increase the frequency selectivity of the filter.

In order to further reveal the device filtering physics, we analyze the normalized magnetic field distributions under TM wave excitation for two different phases of VO_2 in Fig. 4. At the shorter wavelength of 906

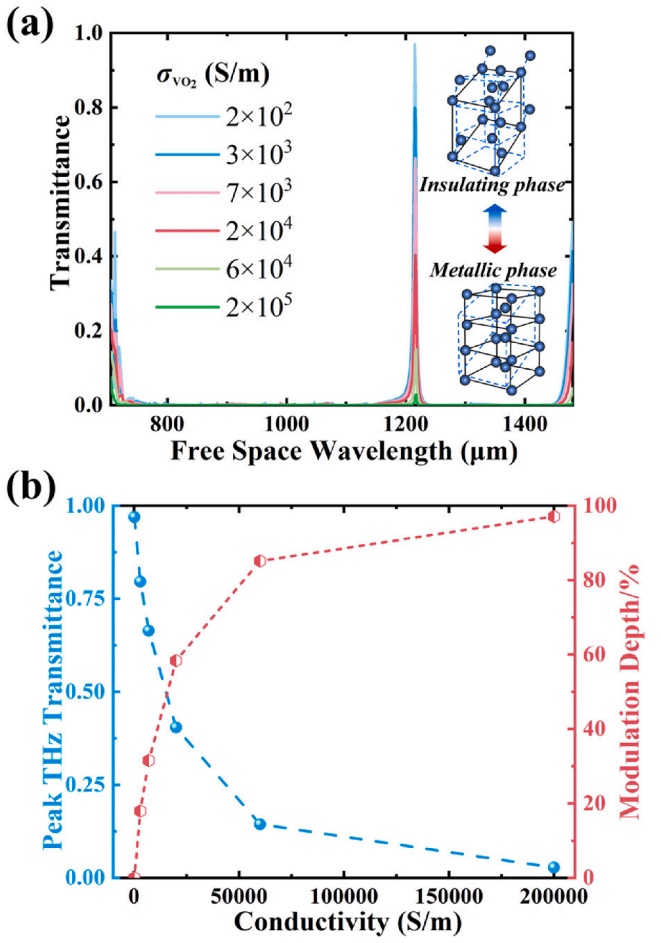

Fig. 5. (a) Transmittance for different conductivities of VO_2. (b) THz transmission peak value as a function of the conductivity of VO_2.

μm, the field distributions are the same for two different VO_2 phases. The THz wave propagates through the CGR and cavity layer, and the field is localized and enhanced within the Si CGR due to its high refractive index. Due to the multiple reflections of the quarter-wave stack, the field amplitude within the DBR is almost zero, which implies that the THz wave is suppressed and cannot penetrate the DBR vertically. At the longer wavelength of 1350 μm, the field distributions for both phases of VO_2 show that the Si CGR has a remarkable optical magnetic field convergence. This could be attributed to the excitation of the guided-mode resonance of the high-index Si CGR, which supports perfect wideband reflection across the long-wavelength range. The THz wave is blocked into the cavity layer and DBR, and the field amplitude is almost zero. We next investigate the field distributions at the transmission peak of $\lambda = 1220$ μm for both VO_2 phases. For the insulating phase, the field amplitude in the entire structure is much smaller than that in the perfect reflection case. The field phase plane along the negative z- direction suggests that the THz wave propagates through the MM from the top air layer to the bottom air layer. On this condition, the wavelength of 1220 μm is located at the overlap region between the longer-wavelength sideband of DBR and the shorter-wavelength sideband of CGR, as shown in Fig. 3(b). At this wavelength, the impedance of MM is perfectly matched with the air, which leads to the perfect transmission. In contrast, for the metallic phase at $\lambda = 1220$ μm, the field amplitude in the MM is enhanced compared to that of the insulating phase, and the field amplitude in the bottom air layer is almost zero. The result implies that the phase change induces the reflection and the block of the THz wave. Our further calculation indicates that the reflectance is about 45% and the THz absorbance is about 53.4% at $\lambda = 1220$ μm.

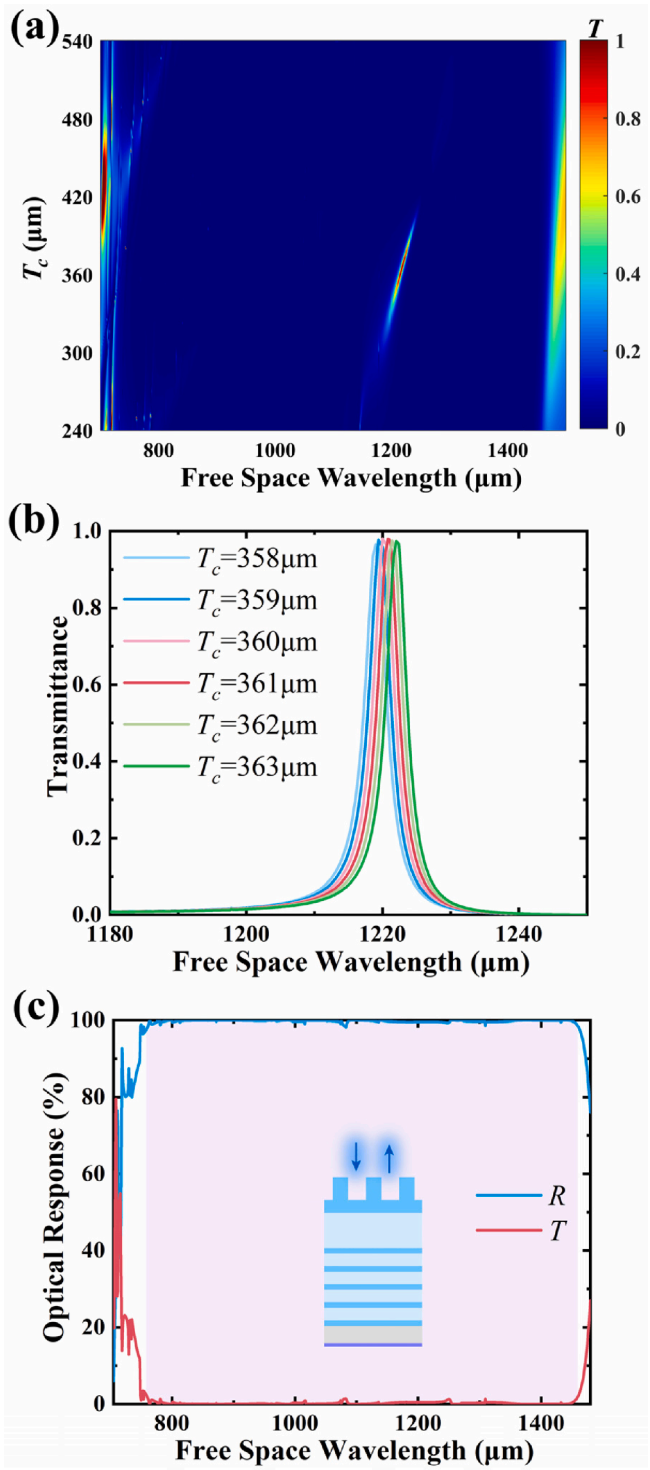

Fig. 6. (a) Transmittance of the THz MM filter as a function of free space wavelength and Topas layer thickness. (b) The zoomed-in image of the transmittance with different T_c. (c) Reflectance and transmittance of the device for the perfect wide reflection band with $T_c = 420$ μm.

To illuminate the device reconfiguration property, we plot the transmittance spectra with the conductivity change of VO_2 in Fig. 5(a). The loss can be introduced by the transition of VO_2 from the insulating monoclinic phase to the metallic rutile phase. One can modulate the transmission intensity by manipulating the thermal excitation on VO_2. The peak transmission and the corresponding modulation depth of the passband derived from Fig. 5(a) are presented in Fig. 5(b). The peak

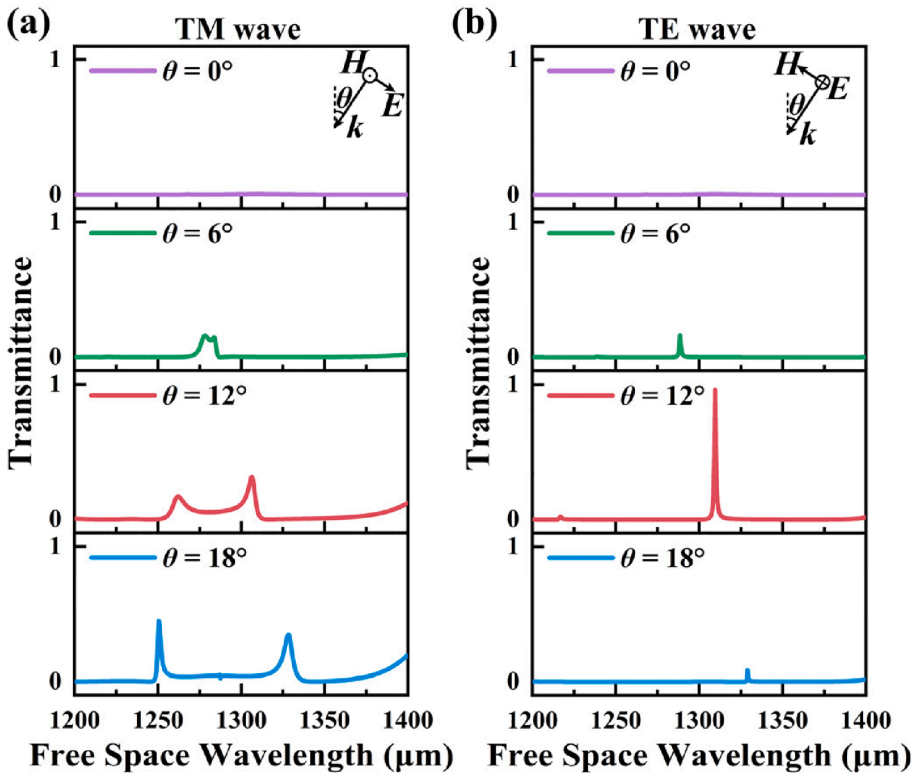

Fig. 7. Transmittance of the device with T_c = 420 μm under different incident angles for (a) TM and (b) TE wave excitation, respectively.

transmittance changes from $T = 96.9\%$ at 2×10^2 S/m to $T = 2.7\%$ at 2×10^5 S/m. According to Equation (3), the maximum modulation depth is 94.2%. The modulating capability of the device is attributed to the IMT features of VO_2.

We perform a detailed investigation of the influence of the cavity layer thickness (T_c) on the filtering performance when VO_2 is in the insulating phase. The introduction of the low-index cavity layer between the CGR and DBR can tune the coupling and create the photonic bandgap, allowing the optical tunneling with a high-Q narrow resonance [26,27]. We plot the transmittance of the hybrid structure as a function of the wavelength and T_c in Fig. 6(a). The obtained results illuminate that the central wavelength of the narrow transmission ($T > 50\%$) shifts from 1205 μm to 1235 μm as the layer thickness rises from 338 μm to 391 μm. As the thickness of the cavity layer increases, the photonic oscillation space changes, resulting in the change of the resonant wavelength and transmittance. Remarkably, the transmittance can exceed over 97% when the layer thickness is between 358 μm and 363 μm, as shown in Fig. 6(b). A maximum transmittance of 98% at the central wavelength of 1220 μm for T_c = 360 μm can be observed. Moreover, the switch from a narrowband filter to a wideband reflector can be accomplished by tuning the value of T_c. The reflectance and transmittance spectra of T_c = 420 μm in Fig. 6(c) illustrate that the perfect wideband reflection ($R > 97\%$) is achieved in the wavelength range of 758–1460 μm, which is attributed to the optical reflection properties of the CGR and DBR.

Additionally, the influence of the oblique incidence on the filtering performance of the device is studied. Based on the perfect reflection with the cavity layer thickness T_c set as 420 μm, we perform a series of simulations with different incident angles θ. We find that the impedance matching between the air and the structure is enabled for the perfect transmission by designing a proper θ. Under TM wave excitation, it is unable to achieve impedance matching and perfect transmission by tuning the value of θ, as shown in Fig. 7(a). On the contrary, a sharp transmission peak of 96.2% with narrow bandwidth is obtained under TE wave excitation for $\theta = 12^\circ$, as presented in Fig. 7(b). The result implies that the impedance of the air and the equivalent impedance of the MM are almost perfectly matched at the transmission wavelength of 1310 μm for TE wave excitation. Based on the above discussions about Figs. 6 and 7, we conclude that one can optimize the cavity thickness and incident conditions to reconfigure the device performance of VO_2-based MM filters and reflectors.

Table 1
Performance Comparison between THz VO_2-based metamaterial filters.

Q-factor	Max Transmittance	Modulation Depth	Refs.
1.315	90%	89%	[14]
2	36%	30%	[15]
2.37	85%	84.7%	[16]
1.5	4.1%	4.1%	[19]
6.6	80.6%	80.6%	[20]
273	98%	96.4%	Our work

Finally, the properties of the THz band-pass MM filters based on VO_2 with the center frequencies below 1 THz are summarized in Table 1 to indicate the importance and novelty of the proposed device. It is observed that the Q-factor and modulation of the filter have been greatly improved over previous work. This implies that our design has the potential to develop high-performance active filters.

Conclusion

In summary, we have investigated a reconfigurable high-Q filter based on the dielectric MM with VO_2. The filter has a narrow passband with the ultra-high Q-factor of 273 and high peak transmission exceeding 98% due to the optical tunneling effects. In our proposed design, two different kinds of reflectors are efficiently combined to achieve the transmission, which suppresses undesired electromagnetic responses and increases the frequency selectivity of the filter. The simulation results suggest that the proposed device has good performance, including high transmission at a specific frequency, sharp edges,

adjustable resonant wavelength, good sideband frequency rejection, and large transmission modulation based on VO_2. By changing the thickness of the cavity layer or incident conditions, the functions of the device can be switched between the wideband reflector and narrowband filter. The design will facilitate the development of THz functional devices like narrowband filters, sensors, switches, and modulators.

CRediT authorship contribution statement

Xueying Liu: Methodology, Software, Formal analysis, Validation, Investigation, Data curation, Visualization, Writing – original draft. **Yinong Xie:** Visualization, Investigation. **Wei Chen:** Validation, Investigation. **Sayed Ali Khan:** Writing – review & editing, Data curation, Validation. **Jun Zhou:** Validation, Investigation. **Jinlin Qiu:** Data curation, Validation, Investigation. **Jinfeng Zhu:** Conceptualization, Methodology, Resources, Software, Validation, Formal analysis, Investigation, Visualization, Supervision, Writing – original draft, Writing – review & editing, Project administration, Funding acquisition.

Declaration of Competing Interest

The authors declare that they have no known competing financial interests or personal relationships that could have appeared to influence the work reported in this paper.

Acknowledgments

This work was supported in part by the National Natural Science Foundation of China (U1830116, U2130112, 62175205); in part by the Science Fund for Distinguished Young Scholars of Fujian Province (2020J06009); in part by the Open Fund of State Key Laboratory of Applied Optics (SKLAO2020001A15).

References

[1] Ferguson B, Zhang X-C. Materials for terahertz science and technology. Nat Mater 2002;1(1):26–33.
[2] Mittleman DM, Jacobsen RH, Nuss MC. T-ray imaging. IEEE J Sel Top Quantum Electron 1996;2(3):679–92.
[3] Koenig S, Lopez-Diaz D, Antes J, Boes F, Henneberger R, Leuther A, et al. Wireless sub-THz communication system with high data rate. Nat Photon 2013;7(12):977–81.
[4] Yang X, Zhao X, Yang K, Liu Y, Liu Y, Fu W, et al. Biomedical applications of terahertz spectroscopy and imaging. Trends Biotechnol 2016;34(10):810–24.
[5] Federici JF, Schulkin B, Huang F, Gary D, Barat R, Oliveira F, et al. THz imaging and sensing for security applications – Explosives, weapons and drugs. Semicond Sci Technol 2005;20(7):S266–80.
[6] Song S, Sun F, Chen Q, Zhang Y. Narrow-linewidth and high-transmission terahertz bandpass filtering by metallic gratings. IEEE Trans Terahertz Sci Technol 2015;5(1):131–6.
[7] Jang W-Y, Ku Z, Jeon J, Kim JO, Lee SJ, Park J, et al. Experimental demonstration of adaptive infrared multispectral imaging using plasmonic filter array. Sci Rep 2016;6:34876.
[8] Chiang Y-J, Yang C-S, Yang Y-H, Pan C-L, Yen T-J. An ultrabroad terahertz bandpass filter based on multiple-resonance excitation of a composite metamaterial. Appl Phys Lett 2011;99(19):191909.
[9] Wang QH, Gao BT, Raglione M, Wang HX, Li BJ, Toor F, et al. Design, fabrication, and modulation of thz bandpass metamaterials. Laser Photonics Rev 2019;13(11):22.
[10] Chang C-C, Huang L, Nogan J, Chen H-T. Invited article: narrowband terahertz bandpass filters employing stacked bilayer metasurface antireflection structures. APL Photon 2018;3(5):051602.
[11] Wu DM, Fang N, Sun C, Zhang X, Padilla WJ, Basov DN, et al. Terahertz plasmonic high pass filter. Appl Phys Lett 2003;83(1):201–3.
[12] Pavanello F, Garet F, Kuppam M-B, Peytavit E, Vanwolleghem M, Vaurette F, et al. Broadband ultra-low-loss mesh filters on flexible cyclic olefin copolymer films for terahertz applications. Appl Phys Lett 2013;102(11):111114.
[13] Jepsen PU, Fischer BM, Thoman A, Helm H, Suh J, Lopez R, et al. Metal-insulator phase transition in a VO_2 thin film observed with terahertz spectroscopy. Phys Rev B 2006;74(20):205103.
[14] Hu F, Wang He, Zhang X, Xu X, Jiang W, Rong Qi, et al. Electrically triggered tunable terahertz band-pass filter based on VO_2 hybrid metamaterial. IEEE J Sel Top Quantum Electron 2019;25(3):1–7.
[15] Young-Gyun J, Bernien Hannes, Kyoung Ji-Soo, Park Hyeong-Ryeol, Sun Kim Hyun. Electrical control of terahertz nano antennas on VO_2 thin film. Opt Express 2011;19(22):21211–5.
[16] Shin J-H, Park KH, Ryu H-C. Electrically controllable terahertz square-loop metamaterial based on VO_2 thin film. Nanotechnology 2016;27(19):195202.
[17] Zhu Y, Vegesna S, Zhao Y, Kuryatkov V, Holtz M, Fan Z, et al. Tunable dual-band terahertz metamaterial bandpass filters. Opt Lett 2013;38(14):2382–4.
[18] Wang S, Kang L, Werner DH. Hybrid resonators and highly tunable terahertz metamaterials enabled by vanadium dioxide (VO_2). Sci Rep 2017;7:4326.
[19] Thompson ZJ, Stickel A, Jeong Y-G, Han S, Son BH, Paul MJ, et al. Terahertz-triggered phase transition and hysteresis narrowing in a nanoantenna patterned vanadium dioxide film. Nano Lett 2015;15(9):5893–8.
[20] Zhao S, Hu F, Xu X, Jiang M, Zhang W, Yin S, et al. Electrically triggered dual-band tunable terahertz metamaterial band-pass filter based on Si_3N_4-VO_2-Si_3N_4 sandwich. Chin Phys B 2019;28(5):054203.
[21] Grischkowsky D, Keiding S, Vanexter M, Fattinger C. Far-infrared time-domain spectroscopy with terahertz beams of dielectrics and semiconductors. J Opt Soc Am B: Opt Phys 1990;7(10):2006–15.
[22] Cunningham PD, Valdes NN, Vallejo FA, Hayden LM, Polishak B, Zhou X-H, et al. Broadband terahertz characterization of the refractive index and absorption of some important polymeric and organic electro-optic materials. J Appl Phys 2011;109(4):043505–043505-5.
[23] Carrillo S-G-C, Nash GR, Hayat H, Cryan MJ, Klemm M, Bhaskaran H, et al. Design of practicable phase-change metadevices for near-infrared absorber and modulator applications. Opt Express 2016;24(12):13563–73.
[24] H.A. Macleod, Thin-film optical filters, CRC press2010.
[25] Ko YH, Magnusson R. Wideband dielectric metamaterial reflectors: Mie scattering or leaky Bloch mode resonance? Optica 2018;5(3):289–94.
[26] Yamamoto N, Akahane K, Gozu SI, Ohtani N. All-optical control of the resonant-photon tunneling effect observed in GaAs/AlGaAs multilayered structures containing quantum dots. Appl Phys Lett 2005;87(23).
[27] Jian AQ, Zhang XM. Resonant optical tunneling effect: recent progress in modeling and applications. IEEE J Sel Top Quantum Electron 2013;19(3).